# A geomorphic study of lagoonal landforms

Alessandra Feola, Enrica Belluco, Andrea D'Alpaos, Stefano Lanzoni, Marco Marani, and Andrea Rinaldo

Dipartimento di Ingegneria Idraulica, Marittima, Ambientale e Geotecnica (IMAGE) and International Center for Hydrology "Dino Tonini," University of Padova, Padua, Italy

Received 15 November 2004; revised 2 March 2005; accepted 10 March 2005; published 29 June 2005.

[1] We perform an analysis of the observational morphological structure of a tidal landscape aimed at examining key assumptions on the geomorphological evolution of wetlands, lagoons, estuarine areas and tidal environments in general. The issues addressed pertain to the statistical measures and the morphodynamic implications of topological or metric properties of the observed landforms, in particular their scale-dependent (or invariant) characters that might suggest self-organized dynamical origins. Field surveys and remote sensing are employed here to accurately characterize different morphodynamic features of a lagoonal environment. Of particular novelty and interest is the structure of landscape-forming shear stresses (properly calculated in unchanneled portions of the landscape) which suggests the viability of threshold models of incision for the formation of tidal channel networks. Distinctive geomorphic indicators, suitable for comparative purposes with modeling of the long-term evolution of tidal systems, are also pointed out. We finally discuss space-distributed analyses of ecogeomorphological properties which strongly suggest the dominance of subvertical processes in the control of the distribution of halophytic vegetation, a key morphodynamic factor.

**Citation:** Feola, A., E. Belluco, A. D'Alpaos, S. Lanzoni, M. Marani, and A. Rinaldo (2005), A geomorphic study of lagoonal landforms, *Water Resour. Res.*, *41*, W06019, doi:10.1029/2004WR003811.

## 1. Introduction

[2] The morphology of tidal landscapes is governed by competing dynamical processes operating at comparable temporal and spatial scales [e.g., *Allen*, 2000]. Signatures of competing geomorphic processes are particularly evident in the development of tidal networks controlling hydrodynamics and sediment transport [e.g., *Pestrong*, 1965; *Friedrichs and Perry*, 2001; *Rinaldo et al.*, 1999a, 1999b]. The study of the intertwined structure of channelled and unchanneled portions of the lagoonal landscape is therefore of particular significance to our understanding of major morphodynamic issues [*Marani et al.*, 2003a; *Novakowski et al.*, 2004]. A tidal landscape is typically classified into three morphological structures, distinguished by the ground elevation with respect to hydraulic duty (mean sea level plus the local tidal range): the salt marshes, the tidal flats and the channel networks. Salt marshes are located at an elevation allowing periodic flooding and colonization by rooted halophytic vegetation. Salt marshes define the transition between permanently emerged and submerged environments, and thus the embedded ecological gradients make them the subject of great ecological interest. Tidal flats lie below mean sea level, emerge only during troughs of spring or neap tides and often do not host vegetation. Channel networks comprise relatively large tidal channels and sinuous inner creeks allowing water, sediment and nutrient exchange between flats, salt marshes and the open sea. In salt marshes, halophytic vegetation, i.e., adapted to living in salty and oxygen-poor environments, plays a central role in controlling erosional and depositional processes, (organic and inorganic) soil production processes and the stability of channel shape and migration [e.g., *Redfield*, 1972; *French and Stoddart*, 1992; *French and Spencer*, 1993; *Allen*, 2000]. This paper studies features that relate to all these morphological structures. In particular, it focuses on landform of a set of field sites located in the northern lagoon of Venice (Italy). This microtidal environment has an area of roughly 550 $km^2$ and is characterized by a semidiurnal tidal regime with a range of about ±0.7 m above msl. Maximum recorded storm surge peaked (04/11/66) at +1.94 m amsl Great concerns remain as to the fate of the residual landforms of the lagoon, which motivate the present morphological studies. In particular, we focus our analysis on two different areas. The first one is the San Felice salt marsh, very close to the Lido inlet: it is mainly colonized by four halophytic species, *Spartina maritima*, *Limonium narbonense*, *Sarcocornia fruticosa* and *Juncus* spp., and its elevation ranges from about mean sea level to 0.68 m above msl, with a mean of 0.26 m; its area has slightly increased in the past 30 years (from 522 $m^2$ in 1968 to 546 $m^2$ in 1998). The second area is the Pagliaga salt marsh which is located near the landward boundary of the lagoon. Pagliaga hosts wide areas of *Phragmites australis*, a glycophytic species, and the halophytic species *Spartina maritima*, *Limonium narbonense*, *Sarcocornia fruticosa*, *Juncus* spp., *Halimione portulacoides* and *Puccinellia Palustris*. Its elevation ranges from 0.02 to 0.97 m above msl, with a mean of 0.47, and its total area has remained constant in the past 10 years, while the total length of its


0043-1397/05/2004WR003811$09.00

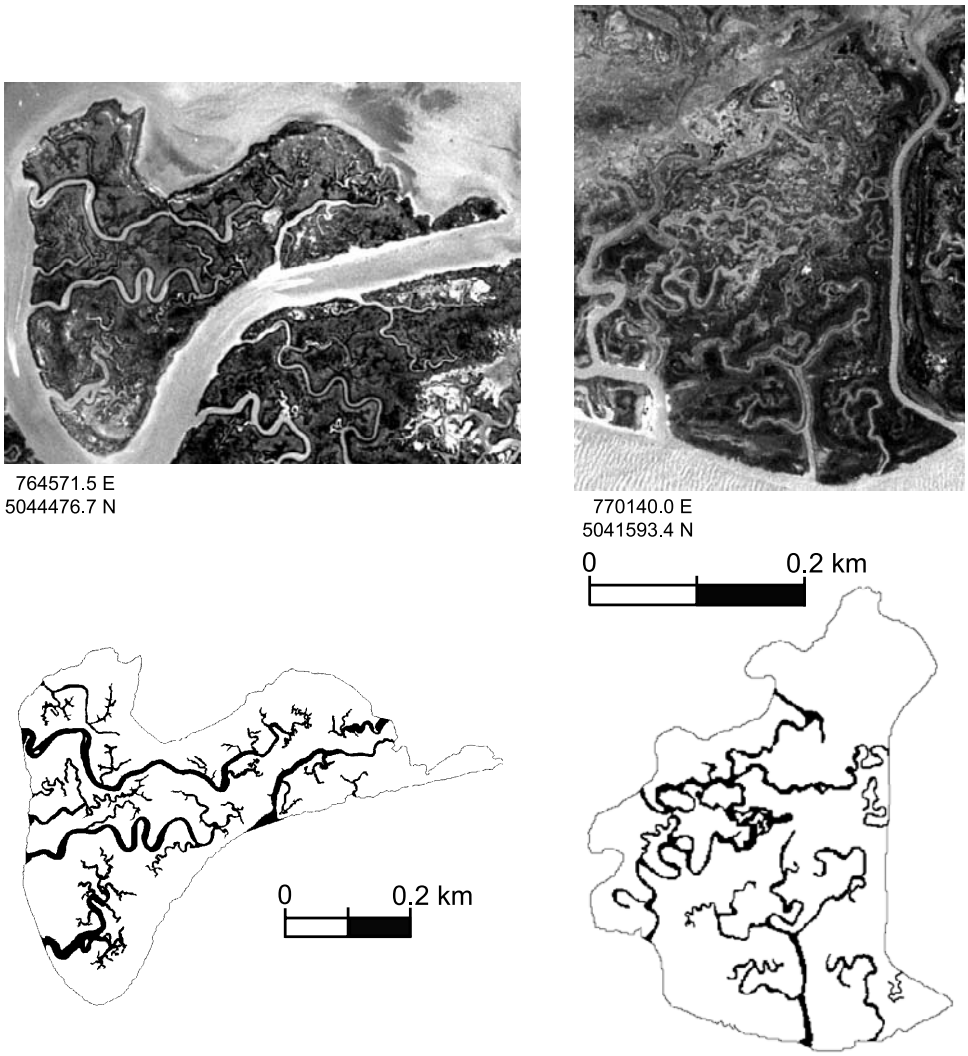


**Figure 1.** Sample of the planar variability of the morphology typical of the salt marshes of the Venice lagoon. For two typical field sites the gray scale aerial photographs together with the extracted channel patterns are shown. The coordinate system is UTM WGS84 fuse 32. Adapted from *Marani et al.* [2003a].

channel network has decreased from 39,500 m in 1987 to 32,800 m in 1996. Soil texture and mechanics vary considerably from one site to the other, in part due to the strong gradients of mean sediment size documented along the general direction from the outlet to the tidal boundary. Further details on the sites considered here are given by *Fagherazzi et al.* [1999] and *Marani et al.* [2002, 2003a].

[3] Remote sensing techniques are an ideal tool for observing tidal environments, typically characterized by difficult accessibility, and allow the objective study of morphological and vegetation patterns over a wide range of spatial scales through accurate and repeatable data acquisition [*Marani et al.*, 2003b, 2004]. We consider here network planforms as extracted from digital aerial photography and their elevation characterization from airborne scanning laser altimetry (0.5 m spatial resolution, vertical accuracy of 15 cm). The distribution of vegetation on the salt marshes, following *Marani et al.* [2003b], is characterized using the CASI airborne hyperspectral sensor (1.3 m ground resolution, 15 spectral bands in the visible and near infrared part of the spectrum, acquisition: 29 September 2002). The accuracy of the remote sensing data was tested by extensive field campaigns performed under the European RTD project TIDE (www.tideproject.org). The extraction of the network was performed either manually, from aerial photograph digitalization and subsequent correction by field survey, or by using semiautomated processing algorithms applied to low-resolution (nonlidar) DEM and lidar data, such as the ones used by *Fagherazzi et al.* [1999]. Algorithms were either based on elevation and curvature thresholds or on the multilevel knowledge-based procedure recently proposed by *Mason and Scott* [2004]. Note that all these techniques allow objective and detailed geomorphological information on tidal channels and creek networks. Two typical examples of aerial photographs of salt marshes analyzed in the Venice lagoon and the corresponding manually extracted networks are shown in Figure 1.

[4] Observed morphological structures show a pattern of spatial gradients typical of tidal landscapes. Network char-

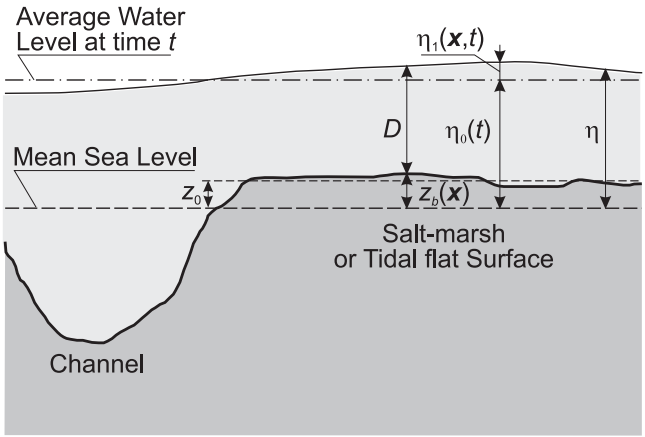


**Figure 2.** Sketch of the transverse profile of an intertidal area. At a given instant $t$ the tidal elevation $\eta(\mathbf{x}, t)$ is given by the sum of its average value in the basin, $\eta_0(t)$, plus fluctuation $\eta_1(\mathbf{x}, t)$, i.e., the local surface elevation above $\eta_0$. The water depth on the salt marsh, $D$, is given by the difference between $\eta$ and the bottom elevation, $z(\mathbf{x})$, both referenced to the mean sea level. Adapted from *Rinaldo et al.* [1999a].

acteristics, in fact, appear to vary not only from one salt marsh to another, but also within distances of a few hundred meters, especially in terms of drainage density [*Marani et al.*, 2003a] and meander sinuosity [*Marani et al.*, 2002]. Such variability suggests the need for combined analysis of physical and ecological processes to address the complex spatial patterns of channelled structures, topography and distribution of vegetation [*Marani et al.*, 2004]. This paper addressed these issues and is organized as follows. Section 2 discusses, after a brief summary of methodological framework, the nearly complete lack of scaling features observed in the tidal systems examined. Section 3 then addresses the spatial variability of geomorphic features, suggesting a locally adapted evolution which involves morphological adjustments to chief land-forming events mainly driven by local hydrodynamics. Physical measures of ecogeomorphological diversity are discussed in section 4, and conclusions are given in section 5.

## 2. Drainage Directions, Gradients of Free Surfaces, and Bottom Shear Stresses

[5] We use tools developed for the analysis of digital terrain maps (DTMs) of fluvial systems, extended to tidal systems in which drainage directions are determined by local gradients of water surfaces rather than by topography. To this end a suitably simplified hydrodynamic model allows one to reduce the two-dimensional shallow water equations of continuity and momentum to a Poisson equation by assuming that tidal propagation is frictionally dominated and that, at time $t$, spatial variations of both water surface and bottom elevations on unchanneled areas (i.e., on salt marshes and tidal flats) are smaller than flow depth. The basic mathematical formulation thus becomes

$$\nabla^2\eta_1 = \frac{\lambda}{(\eta_0 - z_b)^2}\frac{\partial\eta_0}{\partial t}, \qquad \lambda = \frac{8}{3\pi}\frac{U}{\chi^2} \tag{1}$$

where, as shown in Figure 2, $\eta_0(t)$ is the mean water surface elevation (computed with respect to mean sea level) evaluated at a given instant of time t, $\eta_1(\mathbf{x}, t)$ is the deviation from $\eta_0$ of the water surface elevation, $z_b$ is the average bottom elevation (computed with respect to the mean sea level), and $\lambda$ is a suitable friction factor arising from Lorentz's linearization of the friction terms in the momentum equations [*Dronkers*, 1964]. In particular, $\lambda$ relies on a meaningful definition of a velocity scale, $U$, and the Chezy hydraulic friction factor, $\chi$.

[6] Further assuming that the tidal wave propagates much faster (i.e., with infinite celerity) through the tidal channel network than on the shallower intertidal flanking areas [*Rinaldo et al.*, 1999a] leads to the following Poisson boundary value problem to be solved at a given instant of time in the flow field domain, $\Gamma$ [*Rinaldo et al.*, 1999b]:

$$\begin{aligned} \nabla^2\eta_1 &= K \text{ on } \Gamma \\ \eta_1 &= 0 \text{ on } \Gamma' \\ \frac{\partial\eta_1}{\partial n} &= 0 \text{ on } \partial\Gamma'' \end{aligned} \tag{2}$$

where $\Gamma'$ and $\partial\Gamma''$ denote the channel network and impermeable boundaries respectively and the term $K$ ($K = [\lambda/(\eta_0 - z_b)^2]\,\partial\eta_0/\partial t$) is computed using the values of $\eta_0$ and $\partial\eta_0/\partial t$ at a given time t.

[7] Note that, assuming an infinite celerity of propagation within the network, i.e., exploiting the physically reasonable hypothesis of a much faster propagation of the tidal wave through the channel network than on the salt marshes, allows one to solve just once the Poisson boundary value problem (equation (2)). As will be discussed below, the relatively small temporal variations actually experienced by water divides support this procedure. It is then possible to define, at a given instant $t$, the main features of the hydrodynamic field over intertidal areas flooded by the tide, chiefly local bottom shear stresses, through local values of $\nabla\eta_1(\mathbf{x})$, as described below. One example of the resulting spatial distribution of water surface elevation is shown in Figures 3a and 3b. Flow directions, defined by $\nabla\eta_1$, can be obtained at any location in the salt marsh along steepest descent directions, as shown in Figure 3c. Subbasins related to any channel cross section are then uniquely identified as the set of points draining through it (see Figure 3d and section 3). Stringent tests of the validity of the embedded approximations and of the robustness of the model were carried out by *Marani et al.* [2003a], who relaxed the hypothesis that the tidal wave instantaneously propagates within the channel network, assuming that the tide propagates in the channels according to the solution of one-dimensional shallow water equations provided by *Dronkers* [1964]. The Poisson boundary value problem was thus solved at various instants, imposing as boundary condition along the channel network the local surface elevation obtained from Dronkers' solution. The time variability of watershed extent and the migration in time of the divides were then evaluated. The results of this time variant watershed delineation, as well as those obtained through the numerical solution of the complete De Sant-Venant shallow water equations, indicate that

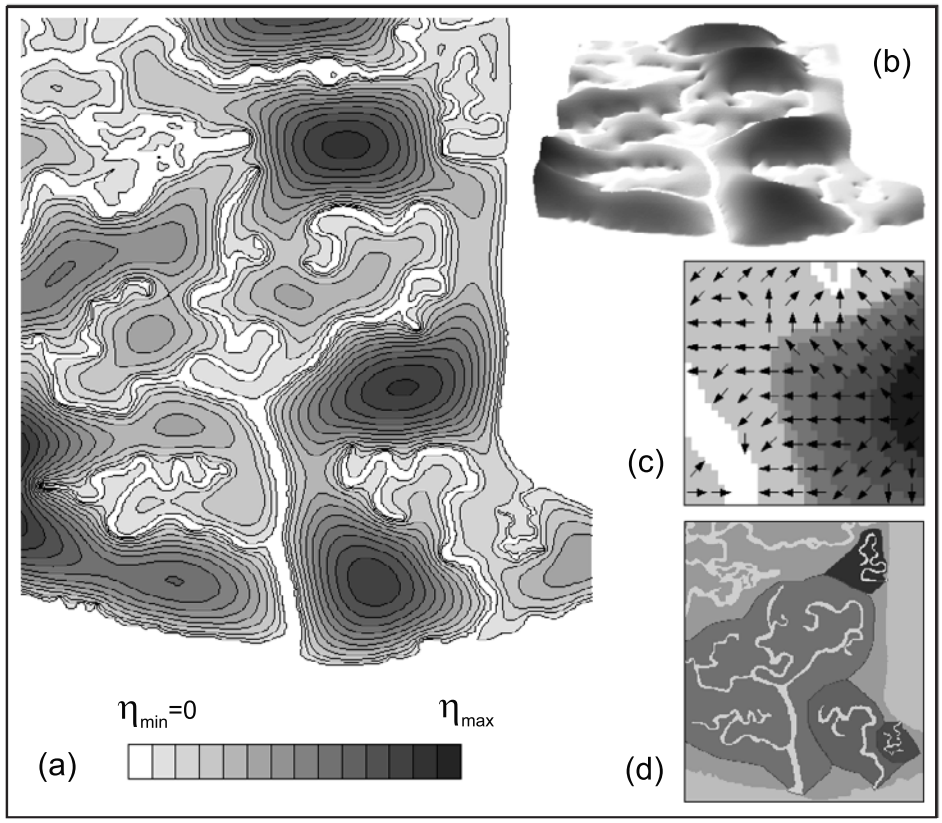


**Figure 3.** Definition of time-averaged features derived from the selection of equation (2): (a) planar and (b) vertically exaggerated three-dimensional views of the water surface elevation $\eta(\mathbf{x}, t^*)$ ($t^*$ is the time of max $\partial\eta_0/\partial t$) for the channel network characterizing the field site of San Felice (Venice), computed by solving the Poisson boundary value problem (equation (2)). The scales ($\eta_{min}$ and $\eta_{max}$) are defined by the tidal range and the relative importance of friction effects within salt marshes. (c) A subset of the drainage directions, uniquely defined by the steepest descent of the water surface topography, which can be computed through the $\eta(\mathbf{x}, t^*)$ field. (d) The watersheds and the drainage areas of subbasin relative to any cross section of the network, which can be delineated through drainage directions.

both in the rising and in the falling phases of the tide, when the maximum flood and ebb discharges are likely to occur, the values of watershed area tend invariably to the solution given by assuming that the tidal wave propagates with infinite celerity through the tidal channel network. This implies that time invariant watershed delineation obtained by solving the boundary value problem just once is suitable.

[8] The simplified Poisson model embodied by equation (2) has already been extensively used to investigate the scaling properties of the tidal networks and the possible empirical relationships relating maximum discharge, cross-sectional channel area, tidal prism, watershed areas, total channel length, over-marsh path lengths (hence drainage densities) to the network and to the divide [*Rinaldo et al.*, 1999a, 1999b; *Marani et al.*, 2003a]. Here we focus our attention on new quantitative measures, relevant to ecomorphodynamical issues.

[9] To analyze where tidal channels begin (or end), reminiscent of analogous concepts in fluvial geomorphology [*Montgomery and Dietrich*, 1988], we have studied the spatial distribution of the shear stresses values $\tau(\mathbf{x})$ acting at the sites on salt marshes or tidal flats adjacent to actual tidal networks. On the basis of the hypotheses used to derive equation (1) it is possible to show that a balance between water surface slope and friction is likely to hold in the momentum equations, which allows one to write

$$\left(\frac{\partial\eta_1}{\partial x}, \frac{\partial\eta_1}{\partial y}\right) = -\frac{1}{\gamma D}(\tau_x, \tau_y) \tag{3}$$

where $(\tau_x, \tau_y)$ denote the local components of the shear stress in the $(x, y)$ directions, $D$ $(=\eta_0 + \eta_1(\mathbf{x}) - z_b(\mathbf{x}))$ is the flow depth, and $\gamma$ is the specific weight of water. Therefore the mean bottom shear stress produced by the tidal flow over the unchanneled portions of tidal basin reads

$$\tau(\mathbf{x}) = \gamma[\eta_0 + \eta_1(\mathbf{x}) - z_b(\mathbf{x})]|\nabla\eta_1(\mathbf{x})| \tag{4}$$

where $\nabla\eta_1(\mathbf{x})$ is the water surface local slope.

[10] One can thus locate and compute the spatial distribution of shear stress values $\tau(\mathbf{x})$ at all intertidal areas and, in particular, in all sites adjacent to the channel network. The results for our case study sites in the Venice lagoon suggest possible general features. In particular a direct inspection of the spatial distribution of $\tau(\mathbf{x})$ indicates that the higher values of the shear stress usually occur at the tips of the channel network and near pronounced channel bends.

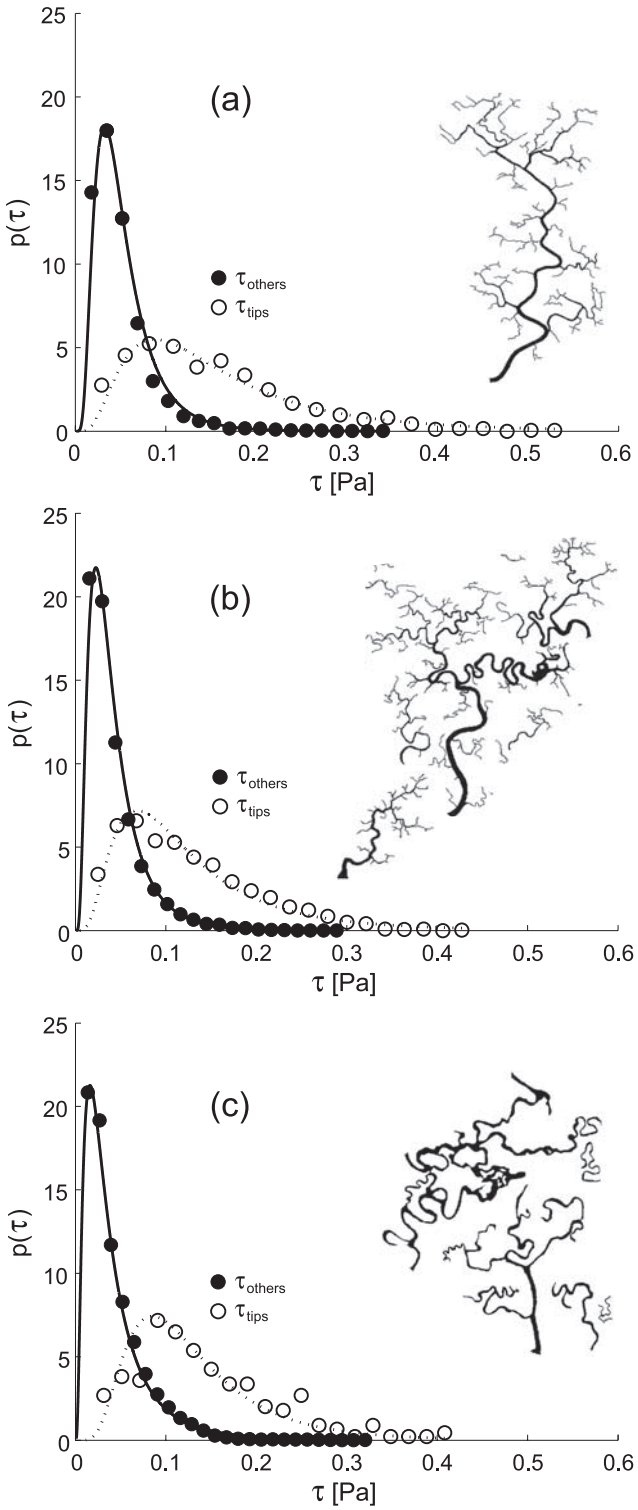


**Figure 4.** Probability density function $p(\tau)$ of the bottom shear stress $\tau(\mathbf{x})$ (equation (4)) both at the tips of the tidal network ($\tau_{tips}$) and at the remaining sites adjacent to it ($\tau_{others}$). Typical salt marshes are sampled. The mean stress value for the investigated zones is (a) Pagliaga, $\bar{\tau} = 0.12$ Pa; (b) Pagliaga sud, $\bar{\tau} = 0.10$ Pa; (c) San Felice, $\bar{\tau} = 0.06$ Pa. Notice that the mean stress reflects the value used for the forcing term $K$ in equation (2). The distributions of $\tau_{tips}$ are consistently peaked at higher values of $\tau$. Notice that the above result would have been strengthened by an ensemble averaging among different sites.

Figure 4 shows three examples of the probability distribution of the shear stresses, $\tau_{tips}$, at the channel heads of a tidal network. The probability density function of shear stresses, $\tau_{others}$, computed for all other adjacent sites with the exception of the tips is also shown in Figure 4. The mean values and the variances of the probability density functions of $\tau_{tips}$ and $\tau_{others}$, indicate that the higher values of the bottom shear stress are usually located at the tips of the channel networks. A similar result is also shown by Figure 5, reporting the spatial distribution of bottom shear stresses computed for all intertidal sites adjacent to the network. Furthermore, Figure 5 suggests that at times, high values of the bottom shear stress arise near channel bends. The fact that higher values of the shear stresses are located near the channel tips, corroborates the speculation that headward erosion and tributary addition (possibly originating at sites where stresses increase along bends) are the main processes of channel elaboration during network development [*Pethick*, 1969; *Steel and Pye*, 1997]. We thus suggest that channel headward growth, guided by the spatial distribution of local shear stresses, is the chief land-forming agent for network formation on real salt marshes. The assumption that erosional activities can be primarily expected in those parts of the landscape where the local value of the bottom shear stress $\tau(\mathbf{x})$ exceeds a threshold value for erosion $\tau_c$ [e.g., *Rinaldo et al.*, 1993, 1995] is found to produce reasonable structures of tidal drainage

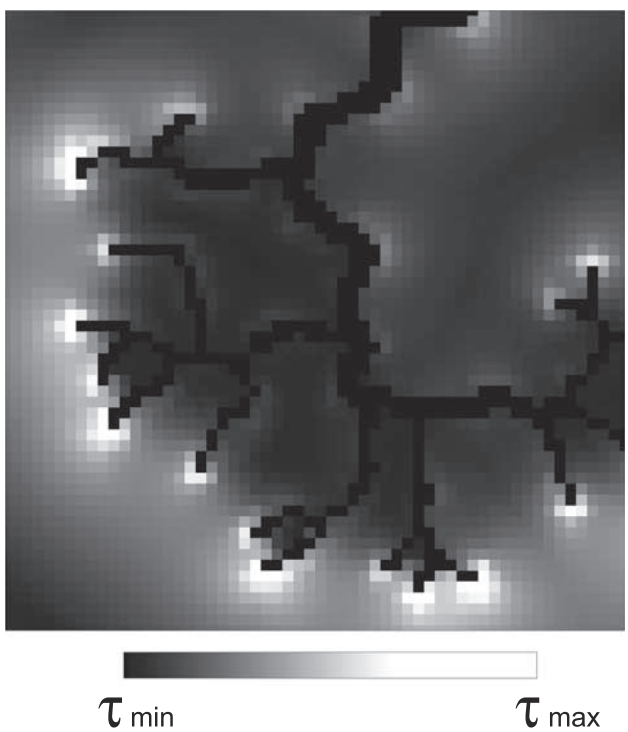


**Figure 5.** Sample of the spatial distribution of the bottom shear stress $\tau(\mathbf{x})$ (equation (4)) attained in intertidal areas in a neighborhood of a specific portion of the network (black pixels). Notice that higher values of the shear stress usually occur at the tips of the channel network and in correspondence to pronounced channel bends. Instead, the higher the local curvature of the tidal channel, the higher the local shear stress in the vicinity.

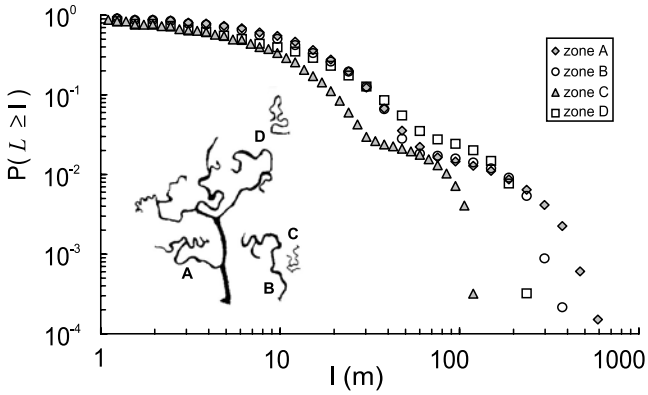


**Figure 6.** Double logarithmic plot of the exceedance probability $P(L \geq l)$ of upstream length, $L$, from every pixel in the basin to the divide, evaluated for four different subbasins in the field site of the San Felice salt marsh.

densities and associated features within tidal landscapes [*D'Alpaos et al.*, 2005].

[11] Obviously, after the initial stages of network formation (which *Allen* [2000] speculates to be quite rapid) subsequent evolution causes the network to become more dense and topologically elaborated as the result of tributary addition and headward growth of its channels [e.g., *Allen* 2000]. Network evolution may also be influenced by other physical mechanisms like tidal meandering [*Marani et al.*, 2002] or, more rarely, channel segmentation resulting from processes like bridging by overhanging vegetation or obstruction by collapsed silt blocks [*Pestrong*, 1972]. Nevertheless, within our field sites, the presence of unconnected tidal channel segments initiated separately from the network and subsequently joined together is rare.

## 3. Scale Dependence in the Tidal Landscape

[12] Flow directions defined by $\nabla\eta_l$ allow for the univocal computation of several metric properties of the tidal landscape like watershed areas, tidal prisms, "upstream" and "downstream" lengths for channelled and unchannelled sites. The use of other nonhydrodynamic procedures to estimate watershed areas, like the one based on Thyssen's polygons adopted by *Novakowski et al.* [2004], introduces an arbitrary source of scatter in the data, though probably not leading to major differences. Likewise, the Hortonian approach to drainage density proves rather elusive, while, on the contrary, the knowledge of the probability distribution of flow lengths from every unchannelled site to the tidal network properly defines the drainage density of the tidal landscape [*Marani et al.*, 2003a].

[13] We describe in the following new analysis of the geometric structure of tidal landscapes based on maps characterized by higher accuracy than the previous data sets used by *Fagherazzi et al.* [1999] and *Rinaldo et al.* [1999a, 1999b]. Probabilities of exceedance of upstream length, $L$, are shown in Figure 6 for the landscape in Figure 1. For every pixel belonging to intertidal areas (unchannelled) or to the network (channelled), $L$ is computed moving along the flow lines, up to the divide of the watershed. The log-log plots of probability density distributions exhibit a departure from power law forms, indicating the presence of characteristic scales of aggregation and hence a markedly different behavior from that observed in river networks [*Rodriguez-Iturbe and Rinaldo*, 1997]. In particular, the probability distribution exhibit two different trends depending on whether $L$ is greater or smaller than 30–70 m.

[14] Further relevant morphological measures may be introduced by computing all downstream unchannelled lengths, $\ell$, evaluated along the flow streamlines determined through the steepest descent direction of the water surface from every unchannelled site (say, over salt marshes or tidal flats) to the nearest channelled point. The unchannelled length $\ell$ is treated as a random space function, thus characterized by progressive moments, as proposed in the context of geomorphology of river basins by *Tucker et al.* [2001] and in tidal environments by *Marani et al.* [2003a]. The properties of the probability density function of this length are in fact physical indices of network capability to drain the basin and thus an appropriate definition of drainage density. The probabilities of exceedance of unchannelled lengths have roughly exponential decays, as shown by the sample semilog plots of Figure 7. Again, the marked differences among the probability distributions for different tidal subbasins, even within the same salt marshes, highlight the strong dependence on site-specific features and competing land-forming processes. A very inhomogeneous drainage density, even within the same salt marsh (the "island" unit according to *Novakowski et al.* [2004]), is therefore obtained. Measures suggesting otherwise (typically the plot of total network length versus watershed area) are deemed inadequate [*Marani et al.*, 2004] and one wonders whether the correlations found by *Novakowski et al.* [2004] by substituting watershed with "island" (i.e., entire salt marsh) area are an artifact of the embedded averaging procedure.

[15] Furthermore, none of the three reasons cited by *Novakowski et al* [2004] to support similarity of fluvial and tidal networks (i.e., (1) the purported topologically random character and the validity of (2) Hack's and (3) Horton's laws)

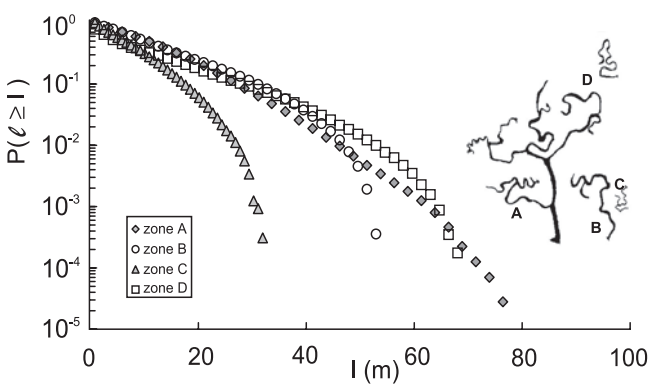


**Figure 7.** Semilogarithmic plot of the exceedance probability $P(\ell \geq l)$ of over-marsh path length, $\ell$, evaluated for four different subbasins in San Felice salt marsh. The marked differences among the exceedance probability distributions, relative to different tidal subbasins, highlight the site-specific character of competing land-forming processes and a very inhomogeneous drainage density even within the same salt marsh.

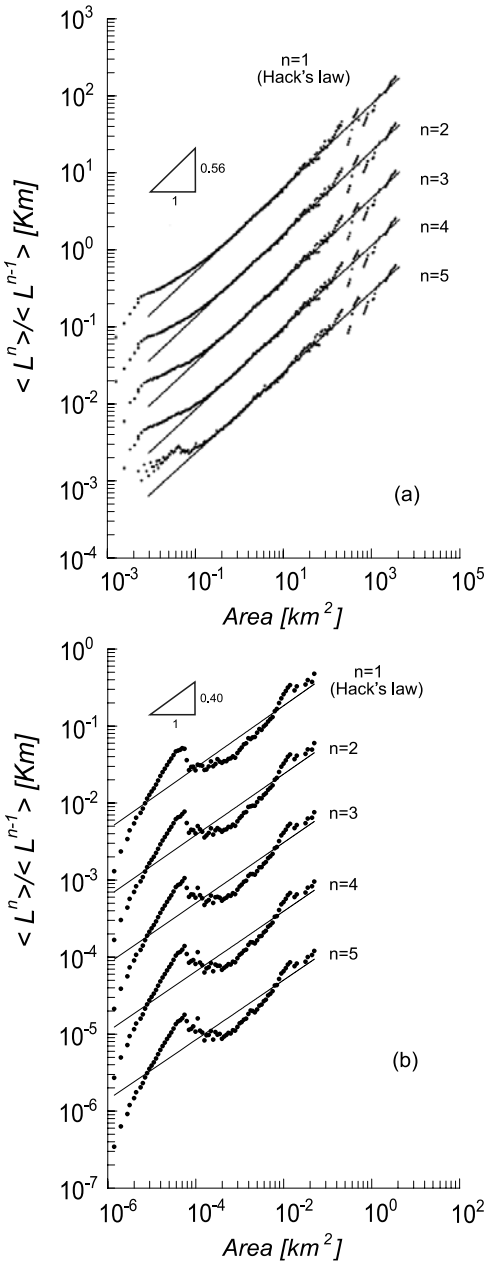


**Figure 8.** Analysis of the scaling of the moments of upstream lengths, $L$, with watershed area, $a$. Double logarithmic plots of the ratios of consecutive moments of the probability distributions of L, relative to points with the same contributing area, are plotted versus $a$ for (a) a fluvial system (after *Rigon et al.* [1996]) and (b) a tidal landscape. A clear straight line across a sizable number of orders of magnitude can be drawn, regardless of the particular moment chosen, only for fluvial systems. On the contrary, in the tidal case, no single power law proves applicable, thereby suggesting that the scaling assumptions do not hold. Other explanations might invoke multiscaling or, simply, no scaling at all [*Rodriguez-Iturbe and Rinaldo*, 1997].

provides a thorough screening. In fact, the topologically random model has been shown to be inconsistent with truly distinctive features of river networks (note for instance that infinite topologically random networks have Hack's exponent exactly equal to 0.5). Moreover, Horton's laws are indistinctive features almost inevitable in tree-like structures [*Kirchner*, 1993].

[16] Rather, we claim that the site specificity and marked heterogeneity that we observe everywhere in the tidal landscape when distinctive geomorphic tools are employed, stems from the pronounced spatial gradients of landscape-forming flow rates and from the imprinting of several interrelated dynamic processes operating at similar spatial scales. We thus further support the claim that tidal landscapes basically differ from tributary morphologies in which fluvial erosion processes predominate across scales.

[17] An important synthesis of the structure of nested subbasins is an empirical law, obtained for fluvial drainage basin [*Hack*, 1957], which is

$$\mathcal{L} \propto \langle L \rangle \sim A^h \tag{5}$$

where $A$ is the total contributing area at any site of a basin and $\mathcal{L}$ is the embedded mainstream length, defined as the longest streamwise distance, measured along the network from the outlet to the watershed divide. $\mathcal{L}$ is obviously proportional to the mean upstream length $\langle L \rangle$.

[18] Hack's "law" has been verified for numerous fluvial drainage basins with excellent fitting throughout several scales. The exponent $h$, typically equal to 0.57, implies an elongation characteristic of fluvial environments. To account for natural variability of river network structures, *Rigon et al.* [1996] have studied the statistical distribution of the upstream length computed by choosing, from each point within the basin, the upstream neighbors with the largest contributing area and iterating until one reaches the divide. Finite size scaling (see, in this context, *Maritan et al.* [1996]) postulates a conditional probability distribution of $L$, relative to a subbasin of area $a$, of the form

$$\pi(L, a) = L^{-\xi} g\left(\frac{L}{L_c(a)}\right) \tag{6}$$

where $L_c(a)$ is a characteristic length and $g(x)$ is a scaling function which takes into account the finite dimension of the network constraining the largest length. By choosing several nested subbasins, one is capable to test the validity of (6) [*Rigon et al.*, 1996]. The argument goes as follows. Through the extension of Hack's law to any single subbasin embedded in a larger basin and to any point on it, the scale length typical of the subbasin, $L_c(a)$, must then be proportional to $a^h$, i.e., $\pi(L, a) \propto L^{-\xi} g(L/a^h)$. By considering the $n$th moment (say $\langle L^n \rangle_a$) of the probability distribution of lengths for all subbasins of area $a$ (whose choice needs suitable binning) and by evaluating the ratios of consecutive moments, *Rigon et al.* [1996] have obtained the result (exact for a distribution like that in equation (6)):

$$\frac{\langle L^n \rangle_a}{\langle L^{n-1} \rangle_a} \propto a^h \tag{7}$$

Notice that for $n = 1$ and $a \equiv A$ one recovers equation (5). This scaling form of the original law allows thorough probing of the resulting aggregation patterns: this is done through the statistical analysis of the ratios of subsequent moments of the probability distributions of upstream length

to the divide, relative to points with the same contributing area. Figure 8a shows the log-log plot of ratios of consecutive moments plotted against the watershed area within a fluvial system. Indeed a clear straight line across a sizable number of orders of magnitude (the signature of a power law) emerges regardless of the particular moment chosen. This is a strong indicator of the validity of the finite size scaling assumption (6) that interprets the Hack's empirical law within a larger, coherent scaling framework. This supports the assumption that the random length from any site to the divide, in a fluvial drainage basin, may be effectively characterized by a probability distribution with a well defined scale-invariant form [*Rodriguez-Iturbe and Rinaldo*, 1997].

[19] We have applied the same analysis to several tidal basins. Interestingly, we find a notable lack of scaling invariance in all tidal embayments regardless of size, tidal range or vegetational properties. Figure 8b shows one example for the landscape in Figure 1 (San Felice, basin A) where the network sites are skeletonized. In contrast with fluvial systems where Hack's exponent describes a good adaptation and consistently falls within a limited range for individual basins, the validity of the adaptation to relationship (equation (7)) is easily denied by any statistical test, as confirmed by visual inspection. Clearly in all tidal networks examined no single power law proves applicable.

[20] Different aggregation regimes are clearly present. The data tends to fall into a nearly straight line only for values of the watershed area lower than $\simeq 5 \cdot 10^{-5}$ Km$^2$. For larger subbasin areas the average slope of the observed data is significantly reduced and no single slope operates for more than a decade. Moreover, large fluctuations appear. This behavior is possibly enhanced by the significant spatial nonstationarity evidenced by Figure 6, which shows that the characteristic unchanneled lengths are different in different regions and in the range $10^1 - 10^2$ m. Note that another embedded characteristic length scale is that of tidal meander wavelengths (or the radius of curvature), which in river basins is typically either absent or, if present, at or below the natural fine scale of the basin description. The ratio $B/R$ of width to radius of curvature is reasonably constant for very different tidal settings, i.e., $B/R = O(10^{-1})$ [*Marani et al.*, 2002]. The resulting length scales affecting aggregation patterns are within the same range of tidal drainage densities ($\approx 10^1 - 10^2$ m of mean unchanneled lengths) and of the networks themselves ($10^2 - 10^3$ m). Roughly unit values of $h$ in unchanneled areas ($\langle L \rangle \propto A$) indicate lack of aggregation, and the elaborate transition to aggregations typical of fluvial networks ($\langle L \rangle \propto A^{0.57}$) (Figure 8b) reflects the overlap of the characteristic scales of meander formation, drainage density establishment and network growth through divide migration. A sharp transition between the two regimes is also prevented by ensemble averaging, which combines site-dependent features. Our analyses of tidal landforms thus suggest that simple geomorphic relationships of the types observed in fluvial basins do not hold throughout the range of scales investigated, and are site-specific.

[21] A word of caution is in order at this point. When analyzing tree-like network structures, one may be misled into finding nonexistent similarities just because the comparison tools are imprecise. This is typically the case with topological measures like Horton's ratios or Tokunaga's matrices and their near inevitability for randomly selected tree-like structures. *Rinaldo et al.* [1998] have shown through exact solutions that similarity of topological measures needs be interpreted only as a necessary condition when comparing network structures. Exactly equal topological structures may lead to very different overall network structures. For example, Peano's basin is very different from natural river basins, nevertheless it is a perfectly Hortonian network, with bifurcation ratio equal to 4 and length ratio equal to 2 and exactly self-similar Tokunaga structure. Thus the common artifact of finding similarity or invariance properties of networks when even visual inspection would have advised otherwise, may depend on the use of non-discriminant topological measures not linked to proper metrics.

## 4. Ecomorphological Measures

[22] The marked scale dependence and site specific features of tidal landscapes revealed by geomorphic measures discussed in sections 2 and 3 suggest the presence of various competing and interrelated processes, acting at overlapping spatial scales. The changes in the morphology of a tidal basin are indeed governed not only by the joint actions of currents generated by tides, wind, and density gradients but also by other factors such as soil topography and type, vegetation species and pattern, biostabilization and bioturbation [*Yallop et al.*, 2000].

[23] Channel geometry is strongly affected by the presence of vegetation in adjacent salt marshes [*Marani et al.*, 2003a, 2004]. The added cohesive properties of the root systems of colonizing halophytic vegetation change the erodibility of channel banks by orders of magnitude [e.g., *Allen*, 2000]. Moreover, the presence of vegetation changes dramatically accretion rates both in terms of organic soil production and sediment trapping [e.g., *French and Spencer*, 1993; *Day et al.*, 1999], and leads to increased frictional resistance to tidal propagation. These effects associated with the presence of vegetation, in turn, often have a significant feedback on hydrodynamics and hence on the general tendency of the tidal embayment to import, export and/or redistribute sediment.

[24] The spatial distribution of halophytic vegetation over salt marshes is not random nor spatially uncorrelated but is, on the contrary, organized in characteristic patches [*Chapman*, 1976; *Bockelmann et al.*, 2002; *Silvestri and Marani*, 2004], whose explanation, in terms of the leading environmental factors affecting it, is relevant for understanding the overall ecomorphological dynamics of tidal systems. Several field studies on salt marshes from different tidal basins show that the distribution of halophytes is strongly correlated to marsh topography and morphology [*Vince and Snow*, 1984; *Adam*, 1990; *Sánchez et al.*, 1996; *Bockelmann et al.*, 2002]. Nevertheless, recent observational and modeling analyses show the existence of marked spatial variability in the relationship between vegetation and topography, which cannot be explained simply in terms of the duration of flooding periods dictated by soil elevation [*Silvestri et al.*, 2005]. The spatial characterization of the organization of different plant species requires objective analyses of observed morphological and vegetation

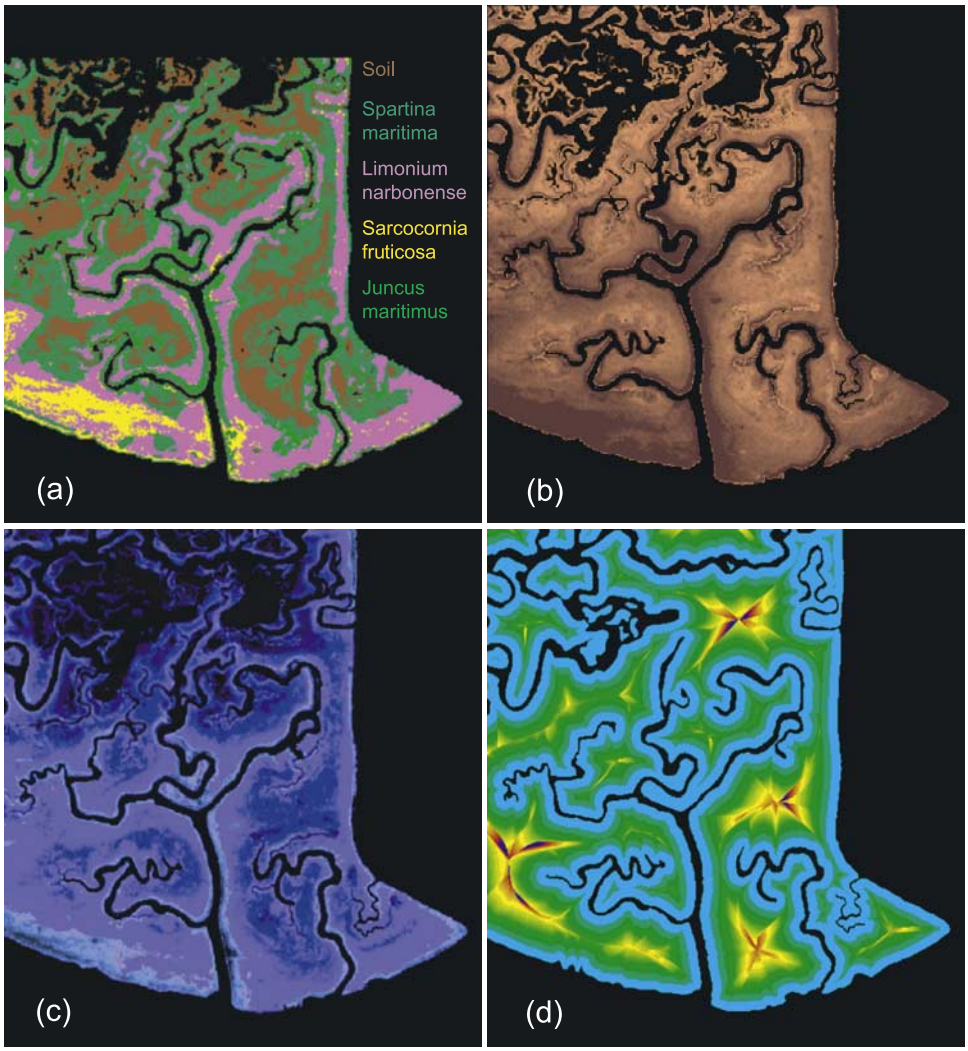


**Figure 9.** Examples of ecogeomorphological measures within San Felice salt marsh: (a) Spatial distribution of halophytic vegetation species resulting from the application to the spectral angle mapping classification algorithm. Six recognizable classes have been considered: (1) *Spartina maritima*, (2) *Limonium narbonense*, (3) *Sarcocornia fruticosa*, (4) *Juncus maritimus*, (5) soil, and (6) water [after *Marani et al.*, 2003b]; (b) spatial distribution of topographic elevation resulting from lidar data; (c) spatial distribution of the hydroperiod, or the submergence ratio, defined as the fraction of the time interval of observation during which a given marsh site is submerged (equation (8)); (d) spatial distribution of unchanneled flow lengths from every site on the salt marshes to the tidal network obtained through steepest descent direction on the average water surface (equations (1) and (2)).

patterns on spatial scales ranging from tens of centimeters to hundreds of meters. *Marani et al.* [2003b] used remote sensing to perform such spatially distributed analyses of vegetation and applied the Spectral Angle Mapper classification schemes [e.g., *Mather*, 1999] to hyperspectral CASI data to retrieve the spatial distribution of halophytes in a number of salt marshes within the Venice lagoon. The spatial distributions of vegetation retrieved from CASI data were found to be consistent with qualitative and quantitative direct observations [*Marani et al.*, 2003b]. Figure 9a shows the results of the classification performed over the San Felice salt marsh (Figure 1) using four vegetation classes representing the four dominant species in the marsh: *Spartina maritima*, *Limonium narbonense*, *Sarcocornia fruticosa*, and *Juncus maritimus* plus one class for water (comprising channels and creeks) and one for bare soil. It well exemplifies the vegetation patterns characteristic of zonation. The spatial distribution of topographic elevation in the same area was achieved from lidar data of the San Felice area (Figure 9b), acquired during low-water stages of the tide, at a flying height of 500 m. Single-pulse data (having a density of 20 returns/m$^2$ and a footprint of 0.17 m) were aggregated at a resolution of $50 \times 50$ cm$^2$, so that the majority of the channels was resolved. The heights in the image range from $-0.1$ m above msl to $+0.7$ m amsl with a nominal error standard deviation of 0.15 m. The patterns of plant zonation and of topographic elevations reported in Figures 9a and 9b are approximately similar thus confirming that processes controlling the spatial organization of halophytic vegetation are strictly related to topography. These results are consistent with point-wise field surveys at several salt marsh locations within the Venice Lagoon, indicating that macrophyte species may be associated with

narrow ranges of soil topographic elevation. The statistical analyses carried out by *Silvestri et al.* [2005] on vegetational and topographic data similar to those reported in Figures 9a and 9b indicate that the frequency distributions of halophytes are sensitive not only to variations in soil elevation, but also to the specific marsh considered. In particular, an identical succession of species with increasing soil elevation was observed in different marshes. However, the range of soil elevations characterizing a given species is dependent on the particular marsh, the plant succession being shifted vertically at different sites [*Silvestri et al.*, 2005]. The presence of different typical elevations for specific plant species in different salt marshes suggests a possible influence exerted by the local value of the hydroperiod [*Kadlec and Knight*, 1996], i.e., the ratio between the time interval during which a given marsh area is submerged to the total duration of the period of reference (e.g., 1 year or the growing season).

[25] Following *Silvestri et al.* [2005], a statistical zero crossing analysis of tidal measurements has been performed to evaluate the hydroperiod at each site of the observed salt marshes, defined as

$$T_h(\mathbf{x}) = \frac{\int_0^{Tr} \mathcal{H}[h(\mathbf{x}, t)]dt}{Tr} \tag{8}$$

where $h(\mathbf{x}, t)$ is the water level at time t in the location $\mathbf{x}$, $\mathcal{H}$ is the Heaviside function (=1 if $h \geq 0$; =0 otherwise) and $T_r$ is the period of interest (one year, or the growing season).

[26] Note that the use of topographic lidar data allows one not only to compute the average value of the hydroperiod characterizing a salt marsh but to extend its evaluation to each salt marsh site, as depicted in Figure 9c.

[27] The comparison between Figures 9c and 9b clearly shows that the hydroperiod correlates with elevation and therefore with zonation (Figure 9a). Although a well-defined, quantitative physical index of vegetation patterning is yet to be devised, nevertheless the relevance of subvertical processes of which elevation is a proxy clearly appears from our data. Indeed, the numerical results recently presented by *Ursino et al.* [2004] emphasize the importance of subvertical processes, such as the interplay between transpiration and infiltration during flooding periods, which affect the persistence of unsaturated zones and, possibly, conditions for oxygen-controlled vegetation.

[28] On the other hand, the patterns of unchanneled flow lengths, computed along flow directions and depicted in Figure 9d, do not show characters relevant to vegetation patterns, in agreement with point-wise observations and previous remote-sensing analyses [*Silvestri et al.*, 2005; *Marani et al.*, 2003b]. Such distances, a proxy for subsurface seepage, approximately coincide with unchannelled distances to the network, because of the relatively small water surface gradient. We thus conclude that horizontal processes do not affect the distribution of vegetation at the marsh scale. This result is in accordance with the numerical studies carried out by *Ursino el al.* [2004] simulating the transient seepage flows induced on a salt marsh by tidal oscillations and the corresponding variation in unsaturated soil moisture. Their results suggest that fluctuations in subsurface flow induced by tidal oscillations in the channel network are dissipated within a distance of a few meters from the channels. Thus the inner salt marsh areas are insensitive to transient seepage and soil moisture dynamics critically depend only on vertical processes.

## 5. Conclusions

[29] 1. The introduction of tidal drainage directions, suitably defined by time-averaged hydrodynamic gradients under a set of assumptions (valid for a reasonably wide spectrum of ebb/fload cases), allows objective definition of tidal watersheds and calculation of a number of geomorphic indicators, chiefly probability distributions of metric and dynamic properties;

[30] 2. Marked scale dependence and site-specific features of tidal landscapes reflect the many conflicting processes that affect the relevant morphodynamics; simple geomorphic relationships of the types observed in the fluvial basin (e.g., power laws for probability density functions of watershed area, upstream length to the divide, unchanneled length to the network) do not hold throughout the actual range of tidal scales and show site-specific characteristics. In particular, Hack's relation, the empirical law of scaling elongation typical of fluvial basin, does not seem to be applicable to tidal networks;

[31] 3. A marked absence of scale-free distributions implies that there is no similarity of the part and the whole within the tidal landscape, in sharp contrast to what happens in fluvial basin where ubiquitous power laws occur. Whereas fluvial systems show various scale-invariant tendencies and dominant processes, mainly of erosive nature, operating across several scales, there seems to be a nearly complete lack of such tendencies in tidal networks owing to competing processes operating at similar spatial scales. Analyses claiming the contrary may indeed have been misled by the subtleties of network comparisons.

[32] 4. Simple morphological indices of ecological diversity suggest the key role of vertical processes in the control of patterns of halophytic vegetation, a key morphodynamic factor of tidal landscapes.

[33] **Acknowledgment.** The financial support of (1) TIDE EU RTD Project (EVK3-CT-2001-00064) (www.tideproject.org) and (2) COFIN 2002 Morfodinamica degli Ambienti a Marea is gratefully acknowledged.

## References

Adam, P. (1990), *Salt-Marsh Ecology*, Cambridge Univ. Press, 461 pp., Cambridge, New York.

Allen, J. R. L. (2000), Morphodynamics of Holocene salt marshes: A review sketch from the Atlantic and southern North Sea coasts of Europe, *Quat. Sci. Rev.*, *19*(17–18), 1155–1231.

Bockelmann, A. C., J. P. Bakker, R. Neuhaus, and J. Lage (2002), The relation between vegetation zonation, elevation and inundation frequency in a Wadden Sea salt marsh, *Aquat. Bot.*, *73*, 211–221.

Chapman, V. J. (1976), *Coastal Vegetation*, 292 pp., 2nd ed., Elsevier, New York.

D'Alpaos, A., S. Lanzoni, M. Marani, S. Fagherazzi, and A. Rinaldo (2005), Tidal network ontogeny: Channel initiation and early development, *J. Geophys. Res.*, *110*, F02001, doi:10.1029/2004JF000182.

Day, J. W., J. Rybczyk, F. Scarton, A. Rismondo, D. Are, and G. Cecconi (1999), Site accretionary dynamics, sea-level rise and the survival of wetlands in Venice lagoon: A field and modelling approach, *Estuarine Coastal Shelf Sci.*, *49*, 607–628.

Dronkers, J. J. (1964), *Tidal Computations*, 518 pp., Elsevier, New York.

Fagherazzi, S., A. Bortoluzzi, W. E. Dietrich, A. Adami, S. Lanzoni, M. Marani, and A. Rinaldo (1999), Tidal networks: 1. Automatic network

extraction and preliminary scaling features from DTMs, *Water Resour. Res.*, *35*, 3891–3904.

French, J. R., and T. Spencer (1993), Dynamics of sedimentation in a tide-dominated backbarrier salt marsh, Norfolk, U.K., *Mar. Geol.*, *110*, 315–331.

French, J. R., and D. R. Stoddart (1992), Hydrodynamics of saltmarsh creek systems: Implications for marsh morphological development and material exchange, *Earth Surf. Processes Landforms*, *17*, 235–252.

Friedrichs, C. T., and J. E. Perry (2001), Tidal salt marsh morphodynamics, *J. Coastal Res.*, *27*, 6–36.

Hack, J. T. (1957), Studies of longitudinal profiles in Virginia and Maryland, *U.S. Geol. Surv. Prof. Pap.*, *294-B*, 45–97.

Kadlec, R. H., and R. L. Knight (1996), *Treatment Wetlands*, pp. 137–140, CRC Press, Boca Raton, Fla.

Kirchner, J. W. (1993), Statistical inevitability of Horton's laws and the apparent randomness of stream channel networks, *Geology*, *21*, 591–594.

Marani, M., S. Lanzoni, D. Zandolin, G. Seminara, and A. Rinaldo (2002), Tidal meanders, *Water Resour. Res.*, *38*(11), 1225, doi:10.1029/2001WR000404.

Marani, M., E. Belluco, A. D'Alpaos, A. Defina, S. Lanzoni, and A. Rinaldo (2003a), On the drainage density of tidal networks, *Water Resour. Res.*, *39*(2), 1040, doi:10.1029/2001WR001051.

Marani, M., E. Belluco, M. Camuffo, A. D'Alpaos, A. Defina, S. Lanzoni, A. Marani, S. Silvestri, and A. Rinaldo (2003b), Patterns in tidal environments: Networks and vegetation, in *IGARSS 2003: Learning From Earth's Shapes and Sizes: 2003 IEEE International Geoscience and Remote Sensing Symposium: Proceedings*, vol. 5, pp. 3269–3271, IEEE Press, Piscataway, N. J.

Marani, M., S. Lanzoni, S. Silvestri, and A. Rinaldo (2004), Tidal landforms, patterns of halophytic vegetation and the fate of the lagoon of Venice, *J. Mar. Syst.*, *51*, 191–210.

Maritan, A., A. Rinaldo, A. Giacometti, R. Rigon, and I. Rodriguez-Iturbe (1996), Scaling in river networks, *Phys. Rev. E*, *53*, 1501–1512.

Mason, D. C., and T. Scott (2004), Remote sensing of tidal channel networks and their relation to vegetation, in *The Ecogeomorphology of Tidal Marshes*, *Coastal Estuarine Stud.*, vol. 59, edited by S. Fagherazzi, M. Marani, and L. K. Blum, pp. 27–46, AGU, Washington, D. C.

Mather, P. M. (1999), *Computer Processing of Remotely-Sensed Images: An introduction*, John Wiley, Hoboken, N. J.

Montgomery, D. R., and W. E. Dietrich (1988), Where do channels begin?, *Nature*, *336*, 232–234.

Novakowski, K. I., R. Torres, R. L. Gardner, and G. Voulgaris (2004), Geomorphic analysis of tidal creek networks, *Water Resour. Res.*, *40*, W05401, doi:10.1029/2003WR002722.

Pestrong, R. (1965), *The Development of Drainage Patterns on Tidal Marshes*, 87 pp., Stanford Univ., Stanford, Calif.

Pestrong, R. (1972), Tidal-flat sedimentation at Cooley Landing, southwest San Francisco Bay, *Sediment. Geol.*, *8*, 251–288.

Pethick, J. S. (1969), Drainage in tidal marshes, in *The Coastline of England and Wales*, 3rd ed., edited by J. R. Steers, pp. 725–730, Cambridge Univ. Press, New York.

Redfield, A. C. (1972), Development of a New England salt marsh, *Ecol. Monogr.*, *24*, 201–237.

Rigon, R., I. Rodriguez-Iturbe, A. Giacometti, A. Maritan, D. Tarboton, and A. Rinaldo (1996), On Hack's law, *Water Resour. Res.*, *32*, 3367–3374.

Rinaldo, A., I. Rodriguez-Iturbe, R. Rigon, R. L. Bras, and E. Ijjasz-Vasquez (1993), Self-organized fractal river networks, *Phys. Rev. Lett.*, *70*, 1222–1226.

Rinaldo, A., W. E. Dietrich, G. Vogel, R. Rigon, and I. Rodriguez-Iturbe (1995), Geomorphological signatures of varying climate, *Nature*, *374*, 632–636.

Rinaldo, A., I. Rodriguez-Iturbe, and R. Rigon (1998), Channel networks, *Annu. Rev. Earth Planet. Sci.*, *26*, 289–327.

Rinaldo, A., S. Fagherazzi, S. Lanzoni, and M. Marani (1999a), Tidal networks: 2. Watershed delineation and comparative network morphology, *Water Resour. Res.*, *35*, 3905–3917.

Rinaldo, A., S. Fagherazzi, S. Lanzoni, M. Marani, and W. E. Dietrich (1999b), Tidal networks: 3. Landscape-forming discharges and studies in empirical geomorphic relationships, *Water Resour. Res.*, *35*, 3919–3929.

Rodriguez-Iturbe, I., and A. Rinaldo (1997), *Fractal River Basins: Chance and Self-Organization*, Cambridge Univ. Press, New York.

Sánchez, J. M., J. Izco, and M. Medrano (1996), Relationships between vegetation zonation and altitude in a salt-marsh system in northwest Spain, *J. Veg. Sci.*, *7*, 695–702.

Silvestri, S., and M. Marani (2004), Salt-marsh vegetation and morphology: Basic physiology, modelling and remote sensing observations, in *The Ecogeomorphology of Tidal Marshes*, *Coastal Estuarine Stud.*, vol. 59, edited by S. Fagherazzi, M. Marani, and L. K. Blum, pp. 5–25, AGU, Washington, D. C.

Silvestri, S., A. Defina, and M. Marani (2005), Tidal regime, salinity and salt-marsh plant zonation, *Estuarine Coastal Shelf Sci.*, *62*, 119–130.

Steel, T. J., and K. Pye (1997), The development of salt marsh tidal creek networks: Evidence from the UK, paper presented at Canadian Coastal Conference, Can. Coastal Sci. and Eng. Assoc., Guelph, Ontario.

Tucker, G. K., F. Catani, A. Rinaldo, and R. L. Bras (2001), Statistical analysis of drainage density from digital terrain data, *Geomorphology*, *36*, 187–202.

Ursino, N., S. Silvestri, and M. Marani (2004), Subsurface flow and vegetation patterns in tidal environments, *Water Resour. Res.*, *40*, W05115, doi:10.1029/2003WR002702.

Vince, S. W., and A. A. Snow (1984), Plant zonation in an Alaskan salt marsh. I. Distribution, abundance and environmental factors, *J. Ecol.*, *72*, 651–667.

Yallop, M. L., D. M. Paterson, and P. Wellsbury (2000), Inter-relationships between rates of microbial production, exopolymer production, microbial biomass and sediment stability in biofilms of intertidal sediments, *Microbial Ecol.*, *39*(2), 116–127.

E. Belluco, A. D'Alpaos, A. Feola, S. Lanzoni, M. Marani, and A. Rinaldo, Dipartimento di Ingegneria Idraulica, Marittima, Ambientale e Geotecnica (IMAGE) and International Center for Hydrology "Dino Tonini", University of Padova, via Loredan 20, I-35131 Padova, Italy. (belluco@idra.unipd.it; adalpaos@idra.unipd.it; feola@idra.unipd.it; lanzo@idra.unipd.it; marani@idra.unipd.it; rinaldo@idra.unipd.it)